3-D Anatomically Based Dynamic Modeling of the Human Knee to Include Tibio-Femoral and Patello-Femoral Joints

Dumitru I. Caruntu
Ph.D.
e-mail: dumitru.caruntu@utoledo.edu

Mohamed Samir Hefzy[1]
Ph.D., P.E.
e-mail: mhefzy@eng.utoledo.edu

Biomechanics and Assistive Technology Laboratory
Department of Mechanical, Industrial and Manufacturing Engineering
The University of Toledo
Toledo, Ohio, USA 43606

An anatomical dynamic model consisting of three body segments, femur, tibia and patella, has been developed in order to determine the three-dimensional dynamic response of the human knee. Deformable contact was allowed at all articular surfaces, which were mathematically represented using Coons' bicubic surface patches. Nonlinear elastic springs were used to model all ligamentous structures. Two joint coordinate systems were employed to describe the six-degrees-of-freedom tibio-femoral (TF) and patello-femoral (PF) joint motions using twelve kinematic parameters. Two versions of the model were developed to account for wrapping and nonwrapping of the quadriceps tendon around the femur. Model equations consist of twelve nonlinear second-order ordinary differential equations coupled with nonlinear algebraic constraint equations resulting in a Differential-Algebraic Equations (DAE) system that was solved using the Differential/Algebraic System Solver (DASSL) developed at Lawrence Livermore National Laboratory. Model calculations were performed to simulate the knee extension exercise by applying non-linear forcing functions to the quadriceps tendon. Under the conditions tested, both "screw home mechanism" and patellar flexion lagging were predicted. Throughout the entire range of motion, the medial component of the TF contact force was found to be larger than the lateral one while the lateral component of the PF contact force was found to be larger than the medial one. The anterior and posterior fibers of both anterior and posterior cruciate ligaments, ACL and PCL, respectively, had opposite force patterns: the posterior fibers were most taut at full extension while the anterior fibers were most taut near 90° of flexion. The ACL was found to carry a larger total force than the PCL at full extension, while the PCL carried a larger total force than the ACL in the range of 75° to 90° of flexion. [DOI: 10.1115/1.1644565]

Introduction

Mathematical knee-joint models have been used to obtain a better understanding of the complicated mechanical behavior of the substructures, which comprise the human musculoskeletal system including the knee joint. Three survey papers [1–3] have appeared during the last decade to review mathematical knee models, which can be classified into either phenomenological or anatomical based models. The later models are more sophisticated and are used to study the behavior of particular structures comprising the human knee. Most of the three-dimensional anatomical based models that were developed to study knee behavior were static or quasistatic, and therefore did not predict the effects of dynamic inertial loads, which occur in many locomotor activities [4–14]. To the best of our knowledge, the model developed by Abdel-Rahman and Hefzy [15] is the only three-dimensional anatomical dynamic model of the knee joint available in the literature. However, Abdel-Rahman and Hefzy's model did not include the patello-femoral joint, nor did it account for deformation of the articular surfaces. The only anatomical dynamic models that include both tibio-femoral and patello-femoral joints are two-dimensional (Tumer and Engin [16] and Ling et al. [17]). The current-state-of-the-art for dynamic knee models differs slightly than that presented in the review conducted by Hefzy and Cooke [3], and can be summarized as follows: *"A single 3-D anatomical dynamic model that includes both tibio-femoral and patello-femoral joints does not yet exist."*

Anatomical based models require an accurate description of the articular surfaces in order to solve the contact problem. Since the dynamic model we propose to develop is by itself an elaborate and computationally demanding model, we will use a simplified contact theory to model the deformable contact at the articular surfaces [18–20]. In this simplified theory, the normal stress between two contacting surfaces is proportional to the shortest penetration distance between these two surfaces.

In this work, we present for the first time the 3-D dynamic response of the knee joint using an anatomical based model that includes three body segments involving both tibio-femoral and patello-femoral joints. The model allows for deformable contact at the articular surfaces and allows for the wrapping of the quadriceps tendon around the femur, which occurs at large flexion angles. Model equations consist of twelve nonlinear second-order ordinary differential equations coupled with nonlinear algebraic constraint equations. To solve this system of equations, the second-order differential equations were transformed into a system of first-order differential equations and then were combined with the algebraic equations to produce a system of Differential Algebraic Equations (DAE). The DAE system is solved by using a DAE solver, namely the Differential/Algebraic System Solver (DASSL) developed at Lawrence Livermore National Laboratory. Model calculations are performed to simulate the knee extension exercise, a commonly prescribed rehabilitation regimen [21]. Nonlinear quadriceps forcing functions with different characteristics were obtained from the experimental data available in the

[1]Corresponding author: Phone: (419) 530.8234; Fax: (419) 530.8206; e-mail: mhefzy@eng.utoledo.edu

Contributed by the Bioengineering Division for publication in the JOURNAL OF BIOMECHANICAL ENGINEERING. Manuscript received by the Bioengineering Division August 20, 2002; revision received August 25, 2003; Associate Editor: C. L. Vaughan.

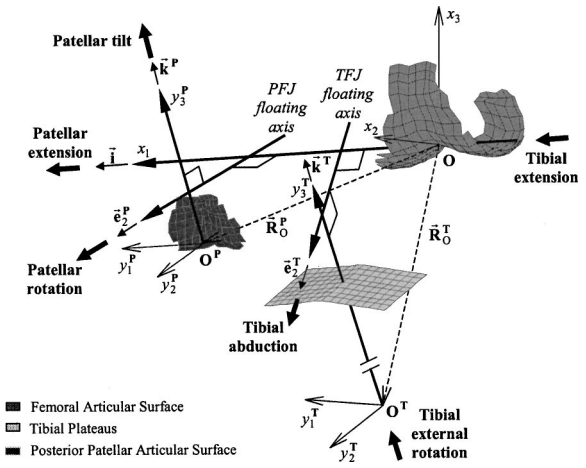

Fig. 1 Tibio-femoral and patello-femoral joint coordinate systems.

literature [22] and used as input to the model. Results are reported to describe the knee response including tibio-femoral and patello-femoral motions and contact forces and anterior and posterior cruciate ligament forces. A comparison of model predictions with related data available in the literature is then presented.

Model Formulation

1 Kinematic Analysis. Three local coordinate systems of axes were identified on the fixed femur and moving tibia and patella as shown in Fig. 1. The tibial and patellar systems were centroidal principal systems of axes, $(y_1^{\mathbf{T}},y_2^{\mathbf{T}},y_3^{\mathbf{T}})$ and $(y_1^{\mathbf{P}},y_2^{\mathbf{P}},y_3^{\mathbf{P}})$, respectively; both of them were parallel to the femoral coordinate system at full extension. The femoral x_1 axis, having $\vec{\mathbf{i}}$ as a unit vector along it, was directed medially for a left knee and laterally for a right knee, and the femoral x_2 and x_3 axes were directed anteriorly and proximally, respectively. The twelve degrees of freedom describing the tibio-femoral joint (TFJ) and the patello-femoral joint (PFJ) motions were defined using two joint coordinate systems [11,15,23], and include 3 rotations and 3 translations for each of the tibial and patellar moving systems. The TFJ $(\vec{\mathbf{i}},\vec{\mathbf{e}}_2^{\mathbf{T}},\vec{\mathbf{k}}^{\mathbf{T}})$ and the PFJ $(\vec{\mathbf{i}},\vec{\mathbf{e}}_2^{\mathbf{P}},\vec{\mathbf{k}}^{\mathbf{P}})$ coordinate systems are identified in Fig. 1; $\vec{\mathbf{k}}^{\mathbf{T}}$ and $\vec{\mathbf{k}}^{\mathbf{P}}$ are two unit vectors along the tibial $y_3^{\mathbf{T}}$ and patellar $y_3^{\mathbf{P}}$ local axes, respectively.

The position vectors of any point on body γ [for tibia: $\gamma=\mathbf{T}$ and for patella: $\gamma=\mathbf{P}$] with respect to the femoral coordinate system and the local body coordinate system, $\vec{\mathbf{R}}^{\gamma}(X_1^{\gamma},X_2^{\gamma},X_3^{\gamma})$ and $\vec{\mathbf{r}}^{\gamma}(x_1'^{\gamma},x_2'^{\gamma},x_3'^{\gamma})$, respectively, are related according to the following transformation:

$$\vec{\mathbf{R}}^{\gamma}=\vec{\mathbf{R}}_{\mathrm{O}}^{\gamma}+[\mathbf{R}^{\gamma}]\vec{\mathbf{r}}^{\gamma} \tag{1}$$

where $\vec{\mathbf{R}}_{\mathrm{O}}^{\gamma}(x_1^{\gamma},x_2^{\gamma},x_3^{\gamma})$ is the position vector of the origin of the γ^{th} body coordinate system with respect to the femoral coordinate system. Equation (1) is written using tensor notation in the following form: $X_i^{\gamma}=x_i^{\gamma}+R_{ij}^{\gamma}x_j'^{\gamma}$, $i,j=1,2,3$, and the (3×3) rotational matrix $[\mathbf{R}^{\gamma}]$ that describes the orientation of the γ^{th} body with respect to the femoral coordinate system is given as:

$$[\mathbf{R}^{\gamma}]=\begin{bmatrix} s_2^{\gamma}c_3^{\gamma} & s_2^{\gamma}s_3^{\gamma} & c_2^{\gamma} \\ -c_1^{\gamma}s_3^{\gamma}-s_1^{\gamma}c_2^{\gamma}c_3^{\gamma} & c_1^{\gamma}c_3^{\gamma}-s_1^{\gamma}c_2^{\gamma}s_3^{\gamma} & s_1^{\gamma}s_2^{\gamma} \\ s_1^{\gamma}s_3^{\gamma}-c_1^{\gamma}c_2^{\gamma}c_3^{\gamma} & -s_1^{\gamma}c_3^{\gamma}-c_1^{\gamma}c_2^{\gamma}s_3^{\gamma} & c_1^{\gamma}s_2^{\gamma} \end{bmatrix}, \quad \gamma=\mathbf{T},\mathbf{P} \tag{2}$$

where $s_k^{\gamma}=\sin\alpha_k^{\gamma}$, $c_k^{\gamma}=\cos\alpha_k^{\gamma}$, $k=1,2,3$. The rotation vectors, $\vec{\boldsymbol{\theta}}^{\mathbf{T}}$ and $\vec{\boldsymbol{\theta}}^{\mathbf{P}}$ describing the orientation of the tibia and patella, respectively, with respect to the femoral coordinate system are thus written as:

$$\vec{\boldsymbol{\theta}}^{\mathbf{T}}=-\alpha_1^{\mathbf{T}}\vec{\mathbf{i}}-\alpha_2^{\mathbf{T}}\vec{\mathbf{e}}_2^{\mathbf{T}}-\alpha_3^{\mathbf{T}}\vec{\mathbf{k}}^{\mathbf{T}}, \quad \vec{\boldsymbol{\theta}}^{\mathbf{P}}=-\alpha_1^{\mathbf{P}}\vec{\mathbf{i}}-\alpha_2^{\mathbf{P}}\vec{\mathbf{e}}_2^{\mathbf{P}}-\alpha_3^{\mathbf{P}}\vec{\mathbf{k}}^{\mathbf{P}} \tag{3}$$

where $\alpha_1^{\mathbf{T}}$ (knee flexion), $\alpha_3^{\mathbf{T}}$ (tibial internal rotation), $\alpha_2^{\mathbf{T}}=(\pi/2\pm\text{Abduction})$, $\alpha_1^{\mathbf{P}}$ (patellar flexion), $\alpha_3^{\mathbf{P}}$ (lateral patellar tilt) and $\alpha_2^{\mathbf{P}}=(\pi/2\pm\text{Patellar lateral rotation})$; a positive sign is used for

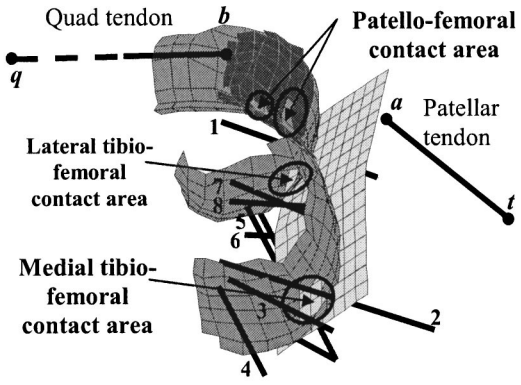

1	LCL	*Lateral Collateral*
2	AMC	*Anterior fibers of the Medial Collateral Ligament*
3	OMC	*Oblique fibers of the Medial Collateral Ligament*
4	DMC	*Deep fibers of the Medial Collateral Ligament*
5	APC	*Anterior fibers of the Posterior Cruciate Ligament*
6	PPC	*Posterior fibers of the Posterior Cruciate Ligament*
7	AAC	*Anterior fibers of the Anterior Cruciate Ligament*
8	PAC	*Posterior fibers of the Anterior Cruciate Ligament*

a, b, q, t — *Apex, basis, femoral quadriceps insertion, tibial tuberosity*

Fig. 2 3-D model of the knee joint (tibio-femoral and patello-femoral joints) showing the collateral and cruciate ligaments

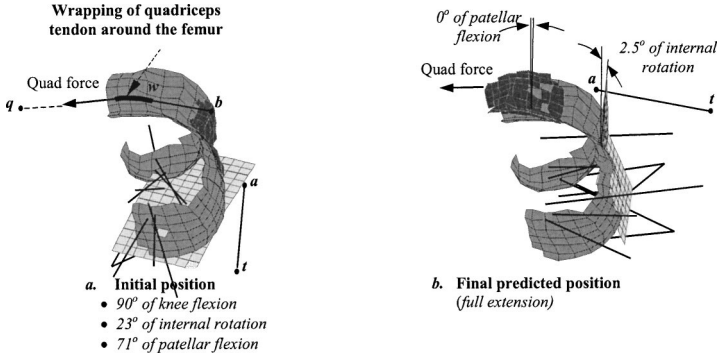

Fig. 3 Initial and final positions during knee extension exercise simulation

the right knee and a negative sign for a left knee [11,15,23]. The relative locations of tibia and patella with respect to the femur, at any position are thus described by **y**, a vector of dimension ($n=12$) consisting of twelve independent kinematic parameters

$$\mathbf{y}=(x_1^{\mathbf{T}},x_2^{\mathbf{T}},x_3^{\mathbf{T}},\alpha_1^{\mathbf{T}},\alpha_2^{\mathbf{T}},\alpha_3^{\mathbf{T}},x_1^{\mathbf{P}},x_2^{\mathbf{P}},x_3^{\mathbf{P}},\alpha_1^{\mathbf{P}},\alpha_2^{\mathbf{P}},\alpha_3^{\mathbf{P}}) \tag{4}$$

2 Mathematical Representation of the Articular Surfaces. The articular surfaces of the distal femur and the posterior patella, along with the planar tibial plateaus were mathematically represented using Coons' parametric bicubic surface patches as shown in Fig. 2. The cartesian coordinates of any point on a surface patch are expressed as bicubic functions of two local parametric coordinates, w_1 and w_2, in the range of 0 to 1 over the patch. These functions were determined in terms of the coordinates of the corner points, which were obtained by digitizing a cadaveric specimen. Details of this mathematical procedure are given by Hefzy and Yang [11].

3 Joint Loads

Quadriceps Tendon Force. Two cases were considered in the analysis to allow for the wrapping (Fig. 3*a*) and nonwrapping (Figs. 2 and 3*b*) of the quadriceps tendon around the femur. For the non-wrapping case, the direction of quadriceps tendon force was assumed parallel to a line of length L^q, joining the patellar basis, point *b*, and the attachment of the quadriceps muscle, point *q*. The components of the quadriceps force expressed in the femoral system, F_i^q, $i=1,2,3$, can thus be written in terms of the six kinematic parameters describing PFJ motions as follows:

$$F_i^q=F^qL_i^q/L^q \tag{5}$$

where F^q is the magnitude of the quadriceps tendon force, $L_i^q=(X_i^q-x_i^{\mathbf{P}}-R_{ij}^{\mathbf{P}}x_j^b)$ are the femoral components of the position vector of point *q* with respect to point *b*, and X_i^q and x_j^b are the components of the local coordinates of points *q* and *b*, respectively.

Wrapping occurs at large flexion angles, normally greater than 70° of knee flexion as shown in Fig. 3*a*. In this situation, the direction of the quadriceps force was assumed parallel to a line of length L^w, joining the patellar basis, point *b*, and the most distal femoral point where wrapping occurs, point *w*, as shown in Fig. 3*a*. The components of the quadriceps force are then expressed as:

$$F_i^q=F^qL_i^w/L^w \tag{6}$$

where $L_i^w=(X_i^w-x_i^{\mathbf{P}}-R_{ij}^{\mathbf{P}}x_j^b)$ are the femoral components of the position vector of point *w* with respect to point *b*, and X_i^w are the femoral coordinates of point *w*. Since point *w* is a point on a femoral patch, its cartesian coordinates, X_i^w, are bicubic functions of its two parametric coordinates, w_1^w and w_2^w. To specify point *w*, two conditions are imposed. First, the plane containing the points *q*, *b* and *w* is assumed parallel to the femoral x_2 axis. Using the scalar triple product this condition is expressed as:

$$\varepsilon_{i2k}L_i^qL_k^w=0 \tag{7}$$

where ε_{i2k} is the alternating tensor. Second, the line L^w (the direction of quadriceps force acting on patella) must be tangent to the femoral surface. This condition is expressed mathematically as:

$$L_i^wN_i^{\mathrm{f}}(w_1^w,w_2^w)=0 \tag{8}$$

where N_i^{f} are the femoral components of unit vector normal to the femoral patch at point *w*.

The components of the moment vector of the quadriceps force around the centroid of the patella, M_i^q, are expressed for both nonwrapping and wrapping cases as follows:

$$M_i^q=\tilde{x}_{ij}^b\mathbf{R}_{kj}^{\mathbf{P}}F_k^q \tag{9}$$

where F_k^q are given by Eq. (5) or (6), and $\tilde{x}_{ij}^b$ are the components of the antisymmetric tensor $[\tilde{x}^b]$ of the local position vector of the patellar basis whose components are x_j^b.

Contact Loads. Friction forces were neglected because of the extremely low coefficient of friction of the articular surfaces [24], and a simplified model was used to allow for a deformable contact at the articulating surfaces of both TFJ and PFJ [18]. While the subchondral bone was assumed to be rigid, the articulating cartilage was considered to be a thin layer of isotropic and linear-elastic material. The normal stress, σ, between two contacting patches located on the moving and fixed surfaces was expressed as $\sigma=Ku$, where u is the penetration, i.e. the total deformation (of both patches) at a contacting point in a direction perpendicular to the moving surface. The contact stiffness, *K*, was calculated as $K=\{[(1-\nu)E]/[(1+\nu)(1-2\nu)t]\}$ where *E*, ν and *t* are the elastic modulus, Poisson's ratio and the thickness of the contacting cartilage layers. By assuming E=5 MPa, $\nu=0.45$ and $t=2$ mm [18], the contact stiffness was calculated as $K=5$ N/mm^3. In this analysis, a uniform stress distribution over each patch was assumed.

An iterative procedure was employed to determine all pairs of contacting patches. Each pair consisted of a source patch located either on tibia or patella and a target patch located on femur. The penetration distance, *u*, was calculated as the projection of a line *ST* onto the normal to the source patch from its center, point *S*. Point *T*, the target point, was identified as the point of intersection of a line drawn from point *S*, and parallel to a specified preferred direction, with the target patch. To calculate TF and PF penetrations, the preferred direction was assumed parallel to the $y_3^{\mathbf{T}}$ tibial axis and the $y_2^{\mathbf{P}}$ patellar axis, respectively. Accordingly, the femoral coordinates of point *T* were calculated using the following two relations:

$$\varepsilon_{ij3}(X_i^T - X_i^S)N_j^d = 0, \quad \varepsilon_{1jk}(X_j^T - X_j^S)N_k^d = 0 \tag{10}$$

where ε_{ijk} is the alternating tensor, N_i^d are the femoral components of a unit vector parallel to the preferred direction, and X_i^T and X_i^S are the femoral coordinates of point *T* and *S*, respectively. In this iterative procedure, the coordinates of point *S* are known. Using the parametric nonlinear equations of the target patches, Eqs. (10) become a nonlinear algebraic system in two unknowns: the parametric coordinates of the target point, w_1^T and w_2^T. The penetration distance between two patches is then calculated using the following relation:

$$u = (X_i^T - X_i^s)N_i \tag{11}$$

where N_i are the femoral components of the outward unit vector normal to the source patch at its center. If u is positive, no contact occurs. The components of the total TF and PF contact forces, F_i^{ct} and F_i^{cp}, respectively, are expressed as:

$$F_i^{ct} = \sum_{m=1}^{M_1} [\sigma_m A_m (N_i)_m]^{ct}; \quad F_i^{cp} = \sum_{m=1}^{M_2} [\sigma_m A_m (N_i)_m]^{cp} \tag{12}$$

where the subscript *m* refers to the *m*th source contacting patch, *A* and σ are the patch area and the patch normal contact stress, respectively, and M_1 and M_2 are the total numbers of the tibial and patellar contacting patches, respectively; superscripts *ct* and *cp* refer to contacting tibial patches within the TFJ and contacting patellar patches within the PFJ, respectively. The components of the total moment vectors of the tibial and patellar contact forces around the tibial and patellar centroids, respectively, are expressed as follows:

$$M_i^{ct} = \mathrm{R}_{kj}^{\mathbf{T}} \sum_{m=1}^{M_1} [(\tilde{x}_{ij})_m \sigma_m A_m (N_k)_m]^{ct};$$

$$M_i^{cp} = \mathrm{R}_{kj}^{\mathbf{P}} \sum_{m=1}^{M_2} [(\tilde{x}_{ij})_m \sigma_m A_m (N_k)_m]^{cp} \tag{13}$$

where $\tilde{x}_{ij}$ are the components of the antisymmetric tensor of the local position vector of point *S* of the m^{th} contacting patch described by its components x_i. Equations (10)–(13) show that the contacting forces and their moments are expressed in terms of the twelve kinematic parameters describing TFJ and PFJ motions, and the parametric coordinates of the target points located on the femoral patches that are in contact with either the tibia or the patella.

Ligamentous Forces. Along with the posterior capsule, the lateral and medial collaterals, and the anterior and posterior cruciates were modeled as shown in Fig. 2. Using 12 discrete fiber bundles, these ligamentous structures were represented using nonlinear spring elements whose force-elongation relationships included quadratic and linear regions [15,18] as follows:

$$(F^\ell)^n = \begin{cases} 0, & \varepsilon^n \leqslant 0 \\ (k^q)^n (L^n - L_0^n)^2, & 0 < \varepsilon^n < 2\varepsilon_0 \\ (k^\ell)^n [L^n - (1+\varepsilon_0)L_0^n], & \varepsilon^n \geqslant 2\varepsilon_0 \end{cases}$$

$$n = 1,2,\ldots,12 \tag{14}$$

where ε^n, $(k^q)^n$, $(k^\ell)^n$, L^n and L_0^n are the strain, the stiffness coefficients for the quadratic and linear regions, and the current length and slack length of the n^{th} element, respectively. The linear range threshold was specified as $\varepsilon_0 = 0.03$. The coordinates of the ligamentous insertion points, the different slack lengths and the stiffness coefficients were obtained using Abdel-Rahman and Hefzy's data [15]. The components of the resultant of the ligamentous forces acting on the tibia, F_i^ℓ, expressed in the femoral coordinate system are written as:

$$F_i^\ell = \sum_{n=1}^{12} (F^\ell)^n L_i^n / L^n \tag{15}$$

and the components of the resultant moment about the tibial center of mass of the ligamentous forces, M_i^ℓ, expressed in the tibial coordinate system are expressed as follows:

$$M_i^\ell = \sum_{n=1}^{12} \tilde{x}'^n_{ij} \mathrm{R}_{kj}^{\mathbf{T}} (F_k^\ell)^n \tag{16}$$

where L_i^n are the femoral components of the position vector of the n^{th} ligamentous structure's femoral insertion with respect to its tibial insertion point and expressed as:

$$L_i^n = X_i^n - x_i^{\mathbf{T}} - \mathrm{R}_{ij}^{\mathbf{T}} x'^n_j \tag{17}$$

where X_i^n and x'^n_j are the local coordinates of the femoral and tibial insertion points, respectively, and $\tilde{x}'^n_{ij}$ are the components of the antisymmetric tensor of the local position vector of the tibial insertion of the n^{th} ligamentous structure. Equations (15), (16) and (17) show that F_i^ℓ and M_i^ℓ are explicitly written as functions of the six tibial kinematic parameters.

Patellar Ligament Force. Connecting the tibial tuberosity, point *t* of local coordinates x_j^t, to the patellar apex, point *a* of local coordinates x_j^a, the patellar ligament is modeled as a linear spring whose tensile force is expressed as:

$$F^p = k^p (L^p - L_0^p) \tag{18}$$

where k^p, L^p and L_0^p are the stiffness, the current length and the slack length of the patellar ligament. The stiffness k^p was assumed to have a value of 200 N/mm [25], and the slack length L_0^p was specified to allow a ratio of 0.6 between the patellar ligament force and the quadriceps force at 90° of flexion [11]. The femoral components L_i^p of the position vector of point *a* with respect to point *t* are expressed as:

$$L_i^p = x_i^{\mathbf{P}} + \mathrm{R}_{ij}^{\mathrm{p}} x_j^a - x_i^{\mathbf{T}} - \mathrm{R}_{ij}^{\mathbf{T}} x_j^t \tag{19}$$

The components of the patellar ligament force acting on the tibia and the patella, F_i^{pt} and F_i^{pp}, respectively, with respect to the femoral coordinate system, are then written as;

$$F_i^{pt} = F^p L_i^p / L^p, \quad F_i^{pp} = -F^p L_i^p / L^p \tag{20}$$

Also, the components of the moments of the patellar ligament force around the tibial and the patellar centroids, expressed in the corresponding local coordinate system are written as

$$M_i^{pt} = \tilde{x}_{ij}^t \mathrm{R}_{kj}^{\mathbf{T}} F_k^{pt}, \quad M_i^{pp} = \tilde{x}_{ij}^a \mathrm{R}_{kj}^{\mathbf{P}} F_k^{pp} \tag{21}$$

where $\tilde{x}_{ij}^t$ and $\tilde{x}_{ij}^a$ are the components of the antisymmetric tensors of the local position vectors of the tibial tuberosity and the patellar apex. Equations (18)–(21) indicate that the patellar ligament force and its moments around the patellar and tibial centroids are explicitly written in terms of the local coordinates of points *t* and *a*, and the twelve motion parameters, $x_i^{\mathbf{T}}$ and $\alpha_i^{\mathbf{T}}$, and $x_i^{\mathbf{P}}$ and $\alpha_i^{\mathbf{P}}$, describing PFJ and TFJ motions, respectively.

4 Equations of Motion. Three Newton and three Euler equations are written for each of the moving tibia and patella, resulting in a system of 12 differential equations of the second order that describes patello-femoral and tibio-femoral motions. Newton equations are written with respect to the fixed femoral coordinate system of axes as (superscript T for tibia and P for patella):

$$W_i^{\mathbf{T}} + F_i^{ct} + F_i^{pt} + F_i^\ell - m^{\mathbf{T}} \ddot{x}_i^{\mathbf{T}} = 0, \quad i = 1,2,3 \tag{22}$$

$$W_i^{\mathbf{P}} + F_i^{cp} + F_i^{pp} + F_i^q - m^{\mathbf{P}} \ddot{x}_i^{\mathbf{P}} = 0, \quad i = 1,2,3 \tag{23}$$

where $\ddot{x}_i^{\mathbf{T}}$ and $\ddot{x}_i^{\mathbf{P}}$ are the components of the accelerations of the tibial and patellar centers of masses, respectively, with respect to the fixed femoral coordinate system; $(m^{\mathbf{T}}, W_i^{\mathbf{T}})$ and $(m^{\mathbf{P}}, W_i^{\mathbf{P}})$ are the masses and weights' components of the tibia and the patella, respectively; F_i^{ct}, F_i^{pt} and F_i^{ℓ} are the components of total TFJ contact force, the patellar ligament force and the resultant of the ligamentous forces, respectively, all acting on the tibia; F_i^{cp}, F_i^{pp} and F_i^{q} are the components of the total PFJ contact force, the patellar ligament force and the quadriceps force, respectively: all acting on the patella.

Euler equations are written in terms of the local tibial and patellar centroidal principal coordinate systems, $(y_1^{\mathbf{T}}, y_2^{\mathbf{T}}, y_3^{\mathbf{T}})$ and $(y_1^{\mathbf{P}}, y_2^{\mathbf{P}}, y_3^{\mathbf{P}})$, respectively. Using tensor notation, the components of the tibial and patellar angular velocities and angular accelerations vectors, denoted by $\dot{\theta}_i'^{\gamma}$ and $\ddot{\theta}_i'^{\gamma}$, respectively ($\gamma$=T for tibia and γ=P for patella), are expressed, with respect to the respective local principal system of axes as follows:

$$\dot{\theta}_i'^{\gamma} = -\mathrm{R}_{ji}^{\gamma}(\mathrm{U}_{jm}^{\gamma} + \alpha_k^{\gamma}\mathrm{U}_{jk,m}^{\gamma})\dot{\alpha}_m^{\gamma} \tag{24}$$

$$\ddot{\theta}_i'^{\gamma} = -\mathrm{R}_{ji}^{\gamma}(\mathrm{U}_{jm}^{\gamma} + \alpha_k^{\gamma}\mathrm{U}_{jk,m}^{\gamma})\ddot{\alpha}_m^{\gamma} - \mathrm{R}_{ji}^{\gamma}(\mathrm{U}_{jm,p}^{\gamma} + \mathrm{U}_{jp,m}^{\gamma} + \alpha_k^{\gamma}\mathrm{U}_{jk,mp}^{\gamma})\dot{\alpha}_p^{\gamma}\dot{\alpha}_m^{\gamma} \tag{25}$$

where $\mathrm{U}_{jk,m}^{\gamma} = \partial \mathrm{U}_{jk}^{\gamma}/\partial \alpha_m^{\gamma}$ and U_{ij}^{γ} are the components of a transformation matrix $[\mathbf{U}^{\gamma}]$ which are defined using the nomenclature of Eq. (2) as:

$$[\mathbf{U}^{\gamma}] = \begin{bmatrix} 1 & 0 & c_2^{\gamma} \\ 0 & c_1^{\gamma} & s_1^{\gamma}s_2^{\gamma} \\ 0 & -s_1^{\gamma} & c_1^{\gamma}s_2^{\gamma} \end{bmatrix} \tag{26}$$

Euler equations of motion are thus written as:

$$M_i^{ct} + M_i^{pt} + M_i^{\ell} - (I^{\mathbf{T}}\ddot{\theta}'^{\mathbf{T}})_i - \frac{1}{2}\varepsilon_{ijk}[(I^{\mathbf{T}}\dot{\theta}'^{\mathbf{T}})_k\dot{\theta}_j'^{\mathbf{T}} - (I^{\mathbf{T}}\dot{\theta}'^{\mathbf{T}})_j\dot{\theta}_k'^{\mathbf{T}}] = 0, \quad i = 1,2,3 \tag{27}$$

$$M_i^{cp} + M_i^{pp} + M_i^{q} - (I^{\mathbf{P}}\ddot{\theta}'^{\mathbf{P}})_i - \frac{1}{2}\varepsilon_{ijk}[(I^{\mathbf{P}}\dot{\theta}'^{\mathbf{P}})_k\dot{\theta}_j'^{\mathbf{P}} - (I^{\mathbf{P}}\dot{\theta}'^{\mathbf{P}})_j\dot{\theta}_k'^{\mathbf{P}}] = 0, \quad i = 1,2,3 \tag{28}$$

where ε_{ijk} is the alternating tensor; M_i^{ct}, M_i^{pt}, M_i^{ℓ} are the tibial components of the moments about the tibial center of mass of the TFJ contact force, the patellar ligament force and all ligamentous forces, respectively; M_i^{cp}, M_i^{pp} and M_i^{q} are the patellar components of the moments about the patellar center of mass of the PFJ contact forces, the patellar ligament force, and the quadriceps force, respectively; $I_i^{\mathbf{T}}$ and $I_i^{\mathbf{P}}$ are the principal moments of inertia of the leg and patella about their respective centroidal principal axes, respectively. The inertial tibial parameters were specified according to the anthropometric data available in the literature [15] as $m^{\mathbf{T}} = 4.0$ kg, $I_1^{\mathbf{T}} = 0.0672$ kg m^2, $I_2^{\mathbf{T}} = 0.0672$ kg m^2 and $I_3^{\mathbf{T}} = 0.005334$ kg m^2. The inertial patellar parameters were assumed as follows: $m^{\mathbf{P}} = 0.1$ kg, $I_1^{\mathbf{P}} = 0.000015625$ kg m^2, $I_2^{\mathbf{P}} = 0.00003125$ kg m^2 and $I_3^{\mathbf{P}} = 0.000015625$ kg m^2.

Two cases have been identified: wrapping and non-wrapping of the quadriceps tendon around the femur. In the non-wrapping situation, the system of equations to be solved consists of 12 nonlinear second-order differential equations (Eqs. (22), (23), (27), (28) and k_1 nonlinear algebraic equations in $(12+k_1)$ unknowns where $k_1 = 2$ $(M_1 + M_2)$ and M_1 and M_2 are the numbers of the tibial and patellar contacting patches, respectively; for each contacting patch, there are two nonlinear algebraic constraints given by Eq. (10). The unknowns in this DAE system of $(12+k_1)$ equations are the 12 kinematic parameters defined in Eq. (4) and (M_1+M_2) pairs of parametric coordinates (w_1^T, w_2^T) defining the target points on the femoral patches that are in contact with the tibia and patella. This DAE system consists thus of 12 nonlinear differential equations $\mathbf{F}(\mathbf{y}, \dot{\mathbf{y}}, \ddot{\mathbf{y}}, \mathbf{w}, t) = 0$ that can be decomposed into two parts as follows:

$$\mathbf{F}(\mathbf{y}, \dot{\mathbf{y}}, \ddot{\mathbf{y}}, \mathbf{w}, t) = \overline{\mathbf{F}}(\mathbf{y}, \dot{\mathbf{y}}, \ddot{\mathbf{y}}, t) + \tilde{\mathbf{F}}(\mathbf{y}, \mathbf{w}) = 0 \tag{29}$$

and k_1 nonlinear algebraic constraints $\mathbf{G}(\mathbf{y}, \mathbf{w}) = 0$ where $\mathbf{y}$ is a vector of dimension 12 containing the 12 kinematic parameters [see Eq. 4], and $\mathbf{w}$ is a vector of dimension k_1 containing the unknown parametric coordinates defining contact. In Eq. (29) $\dot{\mathbf{y}} = \mathrm{d}\mathbf{y}/\mathrm{d}t$ and $\ddot{\mathbf{y}} = \mathrm{d}\dot{\mathbf{y}}/\mathrm{d}t$.

In the wrapping situation, two additional nonlinear algebraic equations [Eqs. (7) and (8)] are added to the DAE system. The corresponding two additional unknowns are the parametric coordinates of the most distal point on the femur where wrapping of the quadriceps tendon occurs, (w_1^w, w_2^w).

Solution Algorithm

The second-order DAE system is transformed to a first-order system by relating joint motions (kinematic parameters) to their velocities $(\nu_i^{\gamma}, \omega_i^{\gamma})$, $i = 1,2,3$. The resulting DAE system contains 24 first-order ordinary differential equations and k_1 nonlinear algebraic constraints [$k_1 = 2(M_1 + M_2)$ for non-wrapping situation and $k_1 = 2(M_1 + M_2 + 1)$ for the wrapping situation], and can be written as:

$$\mathbf{F}(\mathbf{y}, \dot{\mathbf{y}}, \mathbf{w}, t) = \overline{\mathbf{F}}(\mathbf{y}, \dot{\mathbf{y}}, t) + \tilde{\mathbf{F}}(\mathbf{y}, \mathbf{w}) = 0 \quad [24 \text{ equations}] \tag{30a}$$

$$\mathbf{G}(\mathbf{y}, \mathbf{w}) = 0 \quad [k_1 \text{ equations}] \tag{30b}$$

where $\mathbf{y}$ is a vector of dimension 24 containing the 12 kinematic parameters and their velocities. Functions $\tilde{\mathbf{F}}(\mathbf{y}, \mathbf{w})$ represent the contribution of the contact forces (and the quadriceps force in the wrapping situation) to the equations of motion.

In order to solve the DAE system the time span is divided into time steps. At each time station, t_{n+1}, components of $\dot{\mathbf{y}}_{n+1}$ are approximated in terms of $\mathbf{y}_{n+1}$ and $\mathbf{y}$ at previous time steps using a Backward Differentiation Formula (BDF). The DAE system, defined in Eqs. (30*a*) and (30*b*), is thus transformed to the nonlinear algebraic system:

$$\mathbf{F}(\mathbf{y}_{n+1}, \mathbf{w}_{n+1}, t_{n+1}) = 0 \tag{31a}$$

$$\mathbf{G}(\mathbf{y}_{n+1}, \mathbf{w}_{n+1}) = 0 \tag{31b}$$

A solution of the resulting system for $\mathbf{y}_{n+1}$ and $\mathbf{w}_{n+1}$ is thus obtained evaluating iteratively $\mathbf{y}_{n+1}^{(m+1)}$ and $\mathbf{w}_{n+1}^{(m+1)}$ in two steps. First, $\mathbf{w}_{n+1}^{(m)}$ are calculated by solving the following system of equations:

$$\mathbf{G}(\mathbf{y}_{n+1}^{(m)}, \mathbf{w}_{n+1}^{(m)}) = 0 \tag{32}$$

using the Newton-Raphson iteration method. Next, $\mathbf{y}_{n+1}^{(m+1)}$, the approximation of $\mathbf{y}_{n+1}$ in the $(m+1)$th iteration of a modified differential form of the Newton-Raphson method, is calculated using the following relation:

$$\mathbf{y}_{n+1}^{(m+1)} = \mathbf{y}_{n+1}^{(m)} - c[\mathbf{K}(\mathbf{y}_{n+1}^{(m)}, \mathbf{w}_{n+1}^{(m)}, t_{n+1})]^{-1}\mathbf{F}(\mathbf{y}_{n+1}^{(m)}, \mathbf{w}_{n+1}^{(m)}, t_{n+1}) \tag{33}$$

where $\mathbf{F}$ is defined by Eq. (31*a*), $[\mathbf{K}]$ is defined as [26]:

$$[\mathbf{K}] = \left[\frac{\partial \mathbf{F}}{\partial \mathbf{y}}\right] + b\left[\frac{\partial \mathbf{F}}{\partial \dot{\mathbf{y}}}\right] \tag{34}$$

and b and c are two constants that change with the step size and order of BDF to speed up the rate of convergence.

The Differential/Algebraic System Solver (DASSL), developed by Petzold [27], was used to solve the DAE system given by Eqs. (30*a*). This solver uses a Predictor-Corrector algorithm where starting at time station t_n, a predictor polynomial extrapolates the values of $\mathbf{y}_{n+1}^{(0)}$ and $\dot{\mathbf{y}}_{n+1}^{(0)}$ at time station t_{n+1} based on the values

of $\mathbf{y}$ at earlier time stations. Then a corrector utilizes a BDF to transform (30*a*) into (31*a*). Input to the DASSL includes the initial and final times, t_o and t_F, respectively, and the initial values of $\mathbf{y}$, w and $\dot{\mathbf{y}}$. These values satisfy the DAE system (Eqs. 30) at time $t=t_0$. This was done by assuming initial values of $\mathbf{y}$ at time $t=t_0$, and calculating the initial values of $\mathbf{w}$ and $\dot{\mathbf{y}}$ by solving Eqs. (30*a*) and (30*b*).

User-supplied sub-routines evaluate the load vector $\mathbf{F}(\mathbf{y},\dot{\mathbf{y}},\mathbf{w},t)$ and the stiffness matrix $[\mathbf{K}(\mathbf{y},\dot{\mathbf{y}},\mathbf{w},t)]$. The stiffness matrix $[\mathbf{K}]$ is divided into two parts:

$$[\mathbf{K}(\mathbf{y},\dot{\mathbf{y}},\mathbf{w},t)]=[\overline{\mathbf{K}}(\mathbf{y},\dot{\mathbf{y}},t)]+[\tilde{\mathbf{K}}(\mathbf{y},\mathbf{w})] \tag{35}$$

The stiffness matrix $[\overline{\mathbf{K}}]$, which does not depend on $\mathbf{w}$, was calculated using Eq. (34) employing closed-form analytical expressions. On the other hand, the stiffness matrix $[\tilde{\mathbf{K}}]$, which depends on $\mathbf{w}$ but does not depend on $\dot{\mathbf{y}}$, was determined by approximating the partial derivatives using a backward differentiation formula as follows:

$$\tilde{K}_{ij}(\mathbf{y},\mathbf{w})=\frac{\partial \tilde{F}_i}{\partial y_j}(\mathbf{y},\mathbf{w})\cong\frac{\tilde{F}_i(\mathbf{y},\mathbf{w})-\tilde{F}_i[\mathbf{y}-(\Delta y_j)\mathbf{e}_j,\tilde{\mathbf{w}}]}{\Delta y_j} \tag{36}$$

where the vector $\tilde{\mathbf{w}}$ is found by solving $\mathbf{G}[\mathbf{y}-(\Delta y_j)\mathbf{e}_j,\tilde{\mathbf{w}}]=0$ and $\mathbf{e}_j$ is the j^{th} unit vector of dimension $n=24$, which is expressed as $\mathbf{e}_j=(0,0,\ldots,0,1,0,\ldots 0)$.

Model Calculations

In a test situation a forcing function was applied to simulate a knee extension exercise activity. This dynamic loading was applied to the patella through the quadriceps tendon causing the tibia and patella to undergo 3-D motions while the femur was fixed in a horizontal position. The forcing functions, shown in Fig. 4, were specified according to Grood et al.'s experimental data [22] where the quadriceps force was measured during knee extension. Grood et al. [22] reported that this force had a constant average value of 200 N in the range of 10 to 50 deg of knee flexion. This force reached 345 N at full extension, and was 75 N at 90 deg. In the analysis, this forcing function will be referred to as the 200 N quadriceps force. Two other forcing functions with a similar pattern were employed to simulate higher levels of quadriceps contractions: 400 N and 600 N quadriceps forces. The 400 N and 600 N quadriceps forcing functions were specified such that they had a value of 75 N at 90 deg that increased to 400 N and 600 N, respectively, as the knee extended to 50 deg remained constant until 10°, and increased to 530 N and 735 N, respectively, at full extension.

In this simulation, the tibia and the patella were assumed to begin their motions from rest. The initial position is depicted in Fig. 3*a* and was defined according to the experimental data available in the literature data [10,11,13] by specifying the following

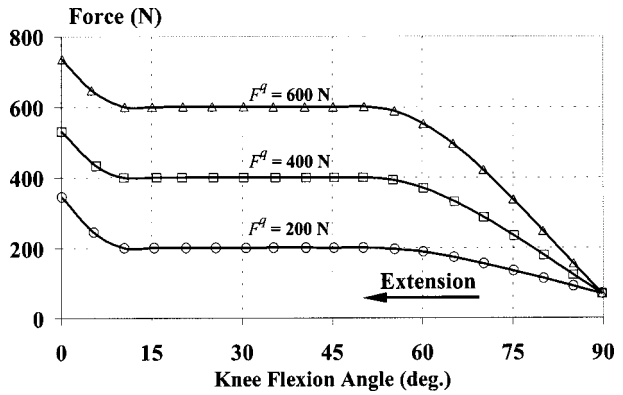

Fig. 4 Forcing functions applied to the quadriceps tendon to simulate knee extension exercise.

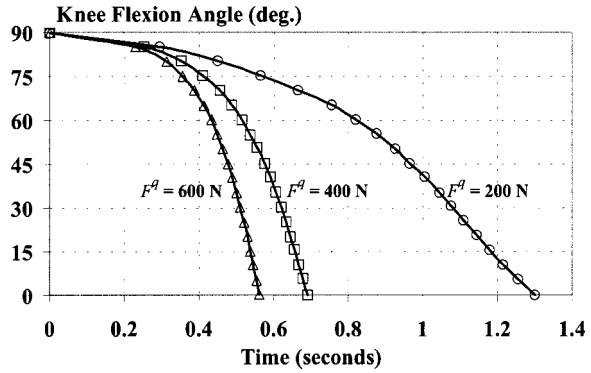

Fig. 5 Duration of knee extension exercise for different quadriceps forcing functions

kinematic parameters: tibial flexion of 89.80 deg, patellar flexion of 71.26 deg, varus (adduction) angle of 4.61 deg, tibial internal rotation of 22.96 deg patellar medial rotation of 0.25 deg, and patellar medial tilt of 0.46°. For each forcing function, and as the simulation progressed from the initial position, the quadriceps tendon continued to wrap around the femur until the flexion angle decreased to a point when wrapping stopped. It was found that the nonwrapping started at 74 deg, 74.14 deg and 74.50 deg of knee flexion for the 200 N, 400 N and 600 N quadriceps forcing func-

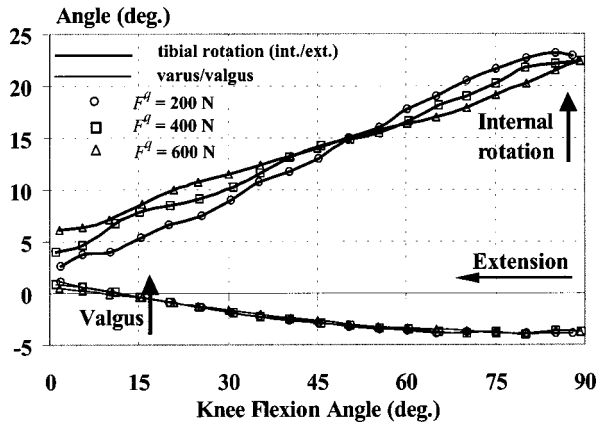

Fig. 6 Internal-external tibial rotations and varus-valgus rotations versus knee flexion angle for different quadriceps forcing functions

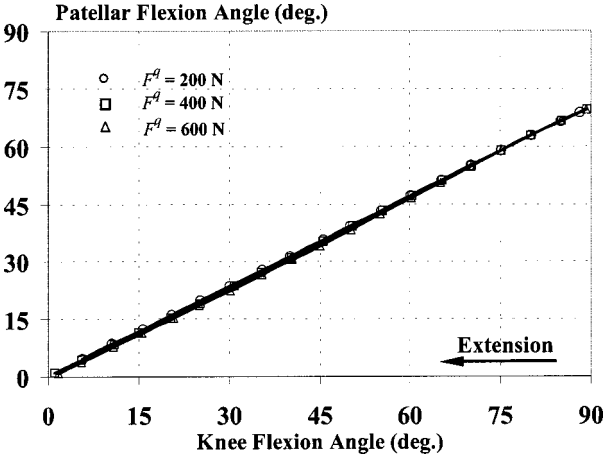

Fig. 7 Patellar flexion angle versus knee flexion angle for different quadriceps forcing functions

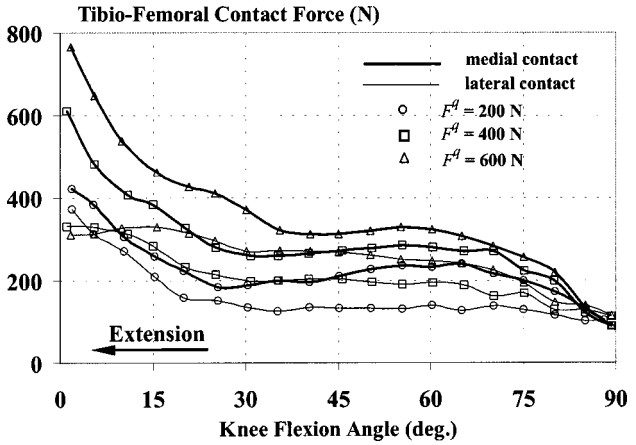

Fig. 8 Medial and lateral components of the tibio-femoral contact force versus knee flexion angle for different quadriceps forcing functions

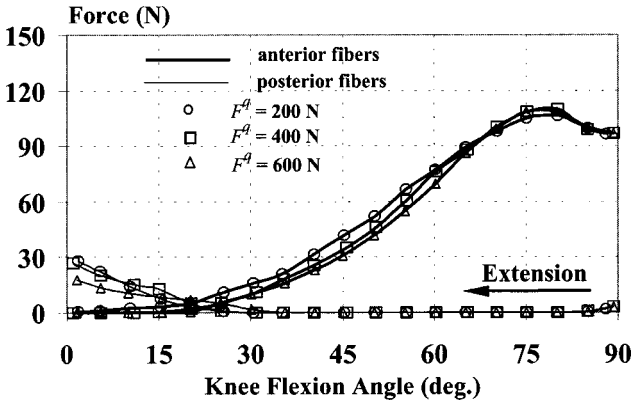

Fig. 11 Forces in the anterior and posterior fibers of the PCL versus knee flexion angle for different quadriceps forcing functions

tions, respectively. The corresponding patellar flexion angles were 57.63, 57.91 and 58.22 deg, respectively. Figure 3*b* shows the predicted final position when the 200 N quadriceps forcing function was used. Figures 3*a* and 3*b* show that with knee extension, the tibia rotated externally (the ''screw home mechanism'') which provides verification for the dynamic simulation. Additional model validation is obtained by studying the changes in the predicted positions of the TF and PF contact with extension. Figures 3*a* and 3*b* show that as the knee was extended, the location of the TF contact moved posteriorly on the medial tibial plateau and anteriorly on the lateral plateau, which reflects an internal rotation of the femur with respect to the tibia (an external rotation of the tibia with respect to the femur). Also, and as expected, the location of the TF contact on the femur moved distally on the condyles. These figures also show that as the knee was extended, the PF contact area moved proximally on the femur. It was also found, as shown in Figs. 2 and 3*b*, that the PF contact moved distally on the patella with knee extension. Fig. 5 shows that the duration of the knee extension exercise decreases as the level of the quadriceps forcing function increases, which also verifies the dynamic analysis. Figure 6 shows that as the tibia was extended from 90° to full extension, it underwent an average of 18.5 deg of external rotation and 4 deg of valgus rotation (abduction). ''Patellar lagging,'' which occurs with knee flexion, was also predicted as shown in Fig. 7.

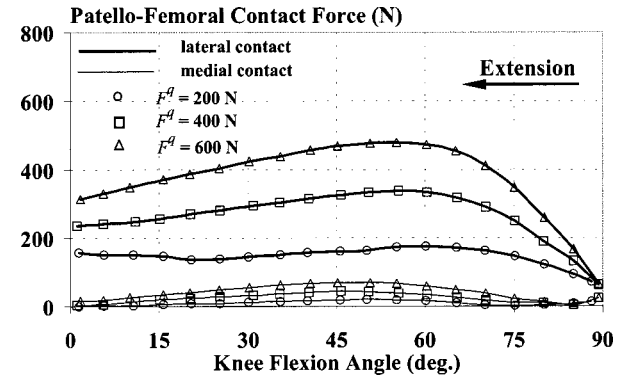

Fig. 9 Lateral and medial components of the patello-femoral contact force versus knee flexion angle for different quadriceps forcing functions

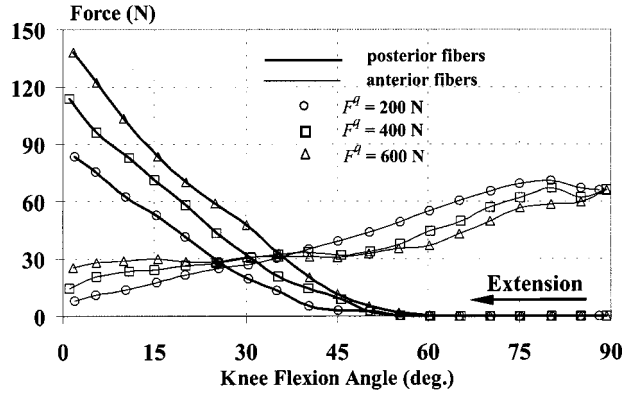

Fig. 10 Forces in the anterior and posterior fibers of the ACL versus knee flexion angle for different quadriceps forcing functions

Figure 8 shows that the medial component of the TF contact force was larger than the lateral component for all tested situations. This figure also shows that the medial component of the TF contact force doubled during the last 30 deg of knee extension, reaching a maximum at full extension. Figure 9 shows that the lateral component of the PF contact force was much larger than its medial component for all tested conditions. Both medial and lateral components of the PF contact force had their largest values in the range of 45 to 60 deg of knee flexion.

Figure 10 shows that as the knee was extended from the 90 deg position to around 35 deg of flexion, the tension in the ACL was greatest in its anterior fibers. As the flexion angle decreased, this tension decreased while tension in the posterior fibers increased and became dominant. Figure 11 shows that the anterior fibers of the PCL carried large forces as the knee was in a flexed position. These forces decreased as the knee was extended. The posterior fibers of the PCL were in tension in the last 10 deg of knee extension. At full extension, the forces in the posterior fibers were greater than those in the anterior fibers, but much smaller than the large forces that were found in the anterior fibers near 90 deg of flexion.

Discussion and Conclusions

A review of the literature reveals that most of the published anatomically based dynamic knee models are 2-D [1–3]. Abdel-Rahman and Hefzy's [15] model is the only anatomical model available in the literature that predicts the three-dimensional dynamic response of the joint under impact loads. Yet, this model was limited in that it was only for the tibio-femoral joint, assumed a rigid contact formulation, and used a spherical representation for the femoral articular surfaces. In this paper, a three-dimensional anatomically based dynamic model of the knee that includes both

tibio-femoral (TF) and patello-femoral (PF) joints is presented. The model allows for deformable contact and for a piecewise mathematical representation of the femoral articular surfaces. The model also allows for wrapping of the quadriceps tendon around the femur that occurs at large flexion angles.

The system of equations forming anatomically based dynamic models is a system of Differential-Algebraic Equations (DAE). Several techniques have been proposed to solve the DAE system that describes the dynamic response of the knee [3]. Most of these techniques were limited in that they could not solve the complicated DAE system that represents the three-dimensional situation. In this paper, the Differential/Algebraic System Solver, DASSL (developed at Lawrence Livermore National Laboratory), was used to solve the complex DAE system to obtain the three-dimensional response of the TF and PF joints under dynamic loading. In order to use this solver, user-supplied subroutines were developed to evaluate the stiffness matrix of the system. Closed-form analytical expressions were written in terms of the kinematic parameters to determine the contributions of the ligamentous and patellar tendon forces, and the quadriceps force in the non-wrapping situation to the stiffness matrix. On the other hand, the contributions of the contact forces and the quadriceps force in the wrapping situation to the stiffness matrix were determined numerically using backward differentiation formulas.

The dynamic response of the knee joint is much different from the static response [28]. Hence, it is hard to compare the present model predictions with similar data reported elsewhere because almost all of the data available in the literature that describes the behavior of the human knee joint are static or quasi-static in nature. In the following, and within these qualifications, model predictions will be discussed and compared with those available in the literature.

The tested condition was used to simulate the knee extension exercise, a common rehabilitation regimen [21]. The forcing functions applied to the quadriceps tendon were specified according to the experimental data available in the literature that quantify quadriceps forces during a knee extension exercise [22].

The classic ''screw-home'' pattern described by many investigators [29] was observed from model predictions. As the knee was extended from 90 deg of flexion to full extension, the tibia rotated externally an average of 18.5 deg. This predicted amount of external rotations is consistent with the experimental values reported in the literature (10 deg by Shoemaker et al. [29], 14.5 deg by Biden et al. [30], 20 deg by FitzPatrick [31], and a range of 14 to 36 deg by Wilson et al. [32]). Model calculations also show that as the knee was extended from 90 deg to about 55 deg of flexion, it did not rotate either in valgus or in varus. As the flexion angle further decreased, the tibia went into valgus (abduction). The dynamic simulation indicated that the tibia was ab-ducted an average of 5 deg as the knee was extended from 55 deg of flexion to full extension. These results are consistent with those reported by Wilson et al. [32] where the authors used two testing conditions (fixed tibia and fixed femur) and 13 knees to describe the knee movements that are coupled with passive knee flexion (no internal-external torques, no varus-valgus torques, no anterior-posterior loads). They reported that as the knee was extended and flexed from a 50 deg of flexion position, it was ab-ducted and ad-ducted on average 5 deg and 1 deg, respectively. They also reported that when the femur was fixed (similar to our numerical simulation), the knee was neither abducted nor adducted as it was flexed from 50 deg to 90 deg of flexion, and was abducted 5 deg as it was extended from 50 to 0 deg of flexion, which is consistent with our model predictions.

Model calculations have also shown that the anterior and posterior fibers of both anterior cruciate ligament (ACL) and posterior cruciate ligament (PCL) had opposite force patterns. The posterior fibers of the ACL were slack in the range of 90 to 60 deg of flexion, and tightened progressively as the knee was extended, reaching a maximum at 0 deg of knee flexion. The anterior fibers

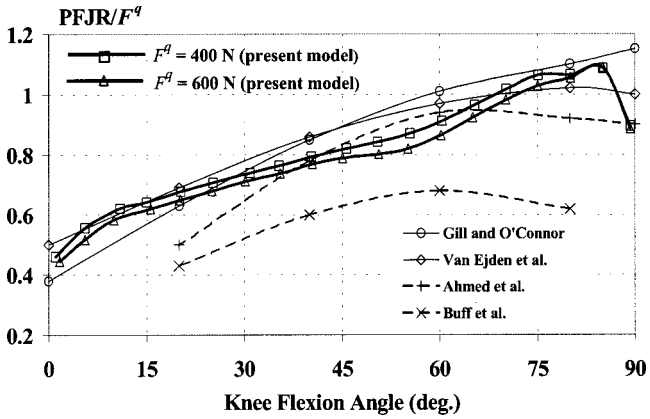

Fig. 12 Ratio of total patello-femoral contact force to quadriceps force versus knee flexion angle: comparison between model predictions and published experimental data and other quasi-static models' predictions

of the ACL were most taut at 90 deg; the tension decreased as the knee was extended. The forces in the anterior fibers of the PCL were large at 90 deg of flexion, increased slightly with knee extension to a maximum around 75 deg, and then decreased progressively until they vanished at 0 deg. On the contrary, the forces in the posterior fibers of the PCL were much smaller: they vanished in the range of 90 to 30 deg and then increased slightly to reach a maximum at 0 deg. These results are in agreement with those reported in the literature to describe the function of the anterior and posterior fibers of both ACL and PCL [33–36].

Model calculations also show that the total force in the ACL (anterior and posterior bundles) reaches a maximum at full extension during the knee extension exercise. At this position, the force in the PCL is comparatively small, which indicates that the ACL carries a larger total force than the PCL at full extension during a knee extension exercise. Also, and in the range of 75 to 90 deg of knee flexion, the forces in the anterior fibers of the PCL (which are maximum) are greater than the forces in the anterior fibers of the ACL (which are also maximum). The posterior fibers of the PCL and the posterior fibers of the ACL do not carry a load in the range of 75 to 90 deg of flexion. These data thus indicate that the total force in the PCL is larger than the total force in the ACL in the range of 75 to 90 deg of flexion. These results are in agreement with Wilk et al.'s data [37] reporting that maximum posterior and anterior tibio-femoral shear forces occurred around 90 and 0 deg of flexion, respectively. This is in agreement with our model calculations since posterior and anterior tibio-femoral shear forces are resisted by the PCL and ACL, respectively. Also, our model calculations have shown that the maximum forces carried by the ACL at full extension are larger than the maximum forces carried by the PCL near 90 deg of flexion. These findings are consistent with other investigators' data reporting that the greatest amount of tibial displacement occurs within the last 30 deg of knee extension during knee extension exercise [22,37–39].

It was also found that the medial component of the tibio-femoral contact force was always larger than the lateral component. It is hard to compare these results with those available in the literature since, and to the best of our knowledge, no data has been reported to compare the medial and lateral components of the tibio-femoral contact force during knee extension exercise. Nevertheless, it has been reported that the medial condyle carries more load than the lateral condyle during a closed chain exercise [40–42].

Model calculations also show that the ratio of the total patello-femoral (PF) contact force to the quadriceps force decreased from nearly 1.1 at 80 deg to 0.45 near full extension as shown in Fig. 12. This is in agreement with other model predictions and with

published data from in vitro studies. Figure 12 shows a comparison between the present model predictions and those of Van Eijden et al.'s [43] and Gill and O'Connor's [44] models, and the experimental data of Ahmed et al. [45] and Buff et al. [46]. Figure 12 shows that the present model predictions are more in agreement with Ahmed et al.'s [45] in vitro study than that of Buff et al. [46].

Model calculations also show that the component of the PF contact force on the lateral side is always greater than the component on the medial side. These results are in agreement with those obtained from the 3-D static models developed by Hefzy and Yang [11] and Hirokawa [14] who has also reported larger contact forces on the lateral side. Also, our model calculations are in agreement with the experimental data available in the literature describing patello-femoral contact. The present results indicate that the contact area on the lateral patellar facet is larger than that on the medial facet at all flexion angles (this is because contact forces are based on contact areas in the present model). This is in agreement with Hille et al. [47], Hefzy et al. [48], and Hehne et al. [49] who have reported larger contact areas on the lateral side. Model calculations have also shown that with knee extension, the location of the PF contact moves proximally on the femur and distally on the patella. These results are in agreement with those reported in the literature describing the locations of the PF contact areas [Hefzy and Yang [11], Hefzy et al. [48]).

Our model calculations also indicate that the pattern that describes how the patello-femoral (PF) contact forces changes with knee flexion depends on the level of quadriceps activation. For large quadriceps forces, the PF contact forces decrease as the knee is extended from 60 deg to full extension. For small quadriceps forces, the PF contact forces remain nearly constant in this range of motion. These data are in agreement with those reported in the literature by Cohen et al. [50] and Takeuchi et al. [51]. During an unloaded open kinetic chain knee extension exercise, Cohen et al. [50] used a quadriceps force with a value of 62 N at 90 deg increasing to 137 N at 60 deg and remaining nearly constant from 60 to 20 deg (no data were reported for lower flexion angles). They reported that the associated PF contact force increased from 120 N at 90 deg to 150 N at 70 deg and remained nearly constant until 20 deg of flexion. Our model predictions show that for a forcing function of $F^q = 200$ N (quadriceps force was 75 N at 90 deg), the total PF contact force increased slightly from 70 N at 90 deg to 175 N at 60 deg then remained nearly constant with further knee extension. A higher and constant quadriceps force of 300 N was used by Takeuchi et al. [51] who reported that for physiologically normal Q-angles, the PF contact forces decreased from 256 N at 60 deg to 143 N at 15 deg of knee flexion. At 90 deg of flexion, they reported a PF contact force of 241 N. Our model calculations show that for a forcing function of $F^q = 300$ N, the PF contact force increased from 70 N at 90 deg to 255 N at 60 deg, then decreased almost linearly to 200 N at 20 deg. The predicted PF contact force has a lower value at 90 deg than that of Takeuchi et al.'s probably because all dynamic quadriceps forcing functions used in this study have a value of only 75 N at this position.

These results suggest that 3-D anatomically based dynamic models of the human musculoskeletal joints are a versatile tool to study the internal forces in these joints. These models are more useful than those less sophisticated quasi-static models, because they can account for the dynamic effects of the external loads. However, the formulation of these dynamic models is critical when it comes to obtaining a solution. The simpler 3-D dynamic model that accounts only for the tibio-femoral joint could not be solved using Moeinzadeh et al.'s formulation [52]. In the formulation presented here, all coordinates of the ligamentous attachment sites were dependent variables that were expressed in terms of the independent kinematic parameters. In addition, these independent kinematic parameters that describe tibio-femoral and patello-femoral motions were used to formulate the wrapping of the quadriceps tendon around the femoral surface and to model the deformable contact at the articular surfaces. As a result, it is possible to introduce more ligaments, to split each ligament into several fiber bundles, to model the wrapping of the quadriceps around the femur that occurs at large flexion angles, and to allow for more or fewer surface patches, as appropriate, to come into contact. This formulation allowed the solution of this intricate 3-D dynamic model.

The present 3-D model can be used to analyze knee response to dynamically applied load, which has particular application to injury mechanics. Since most injuries to the knee involve dynamic loads, this model, which accounts for the inertial effects of those dynamic forces, will provide a valuable tool to study the underlying mechanisms for these injuries. In this model, the menisci were not included and the definition of the tibial articular surfaces was not considered. No distinction was made between the medial and lateral tibial articular surfaces. However, further developments of incorporating the menisci, differentiating between the medial and lateral articular surface geometry, particularly in terms of posterior slope and medio-lateral inclination, and modeling muscular co-contractions will allow the model to be used to study daily living activities where dynamic axial compressive forces act on the joint as in walking and running.

Acknowledgments

This work was supported by grant BES-9809243 from the Biomedical Engineering Program of the National Science Foundation.

References

[1] Hefzy, M. S., and Grood, E. S., 1988, "Review of Knee Models," Appl. Mech. Rev., **41**(1), pp. 1–3.
[2] Hefzy, M. S., and Abdel-Rahman, E. M., 1995, "Dynamic Modeling of the Human Knee Joint: Formulation and Solution Technique. A Review Paper," J. Biomed. Eng.: Application, Basis and Communication, **7**(1), pp. 5–21.
[3] Hefzy, M. S., and Cooke, T. D. V., 1996, "Review of Knee Models: 1996 Update," Appl. Mech. Rev., **49**(10), pp. 187–193.
[4] Donahue, T. L. H., Hull, M. L., Rashid, M. M., and Jacobs, C. R., 2002, "A Finite Element Model of the Human Knee Joint for the Study of Tibio-Femoral Contact," J. Biomech. Eng., **124**, pp. 273–280.
[5] Suggs, J., Wang, C., and Li, G., 2003, "The Effect of Graft Stiffness on Knee Joint Biomechanics after ACL Reconstruction—A 3D Computational Simulation," Clin. Biomech. (Los Angel. Calif.), **18**, pp. 35–43.
[6] Li, G., Suggs, J., and Gill, T., 2002, "The Effect of Anterior Cruciate Ligament Injury on Knee Joint Function under a Simulated Muscle Load: A Three-Dimensional Computational Simulation," Ann. Biomed. Eng., **30**, pp. 713–720.
[7] Liu, W., and Maitland, M. E., 2000, "The Effect of Hamstring Muscle Compensation for Anterior Laxity in the ACL-Deficient Knee During Gait," J. Biomech., **33**, pp. 871–879.
[8] Huss, R. A., Holstein, H., and O'Connor, J. J., 2000, "A Mathematical Model of Forces in the Knee Under Isometric Quadriceps Contractions," Clin. Biomech. (Los Angel. Calif.), **15**, pp. 112–122.
[9] Li, G., Gil, J., Kanamori, A., and Woo, S. L.-Y., 1999, "A Validated Three-Dimensional Computational Model of a Human Knee Joint," J. Biomech. Eng., **121**, pp. 657–662.
[10] Wilson, D. R., Feikes, J. D., and O'Connor, J. J., 1998, "Ligaments and Articular Contact Guide Passive Knee Flexion," J. Biomech., **31**, pp. 1127–1136.
[11] Hefzy, M. S., and Yang, H., 1993, "A Three-Dimensional Anatomical Model of the Human Patello-Femoral Joint, for the Determination of Patello-Femoral Motions and Contact Characteristics," J. Biomed. Eng., **15**, pp. 289–301.
[12] Blankevoort, L., and Huiskes, R., 1996, "Validation of a Three-Dimensional Model of the Knee," J. Biomech., **29**(7), pp. 955–961.
[13] Heegaard, J., Leyvraz, P. F., Curnier, A., Rakotomanana, L., and Huiskes, R., 1995, "The Biomechanics of the Human Patella During Passive Knee Flexion," J. Biomech., **28**(11), pp. 1265–1279.
[14] Hirokawa, S., 1991, "Three-Dimensional Mathematical Model Analysis of the Patellofemoral Joint," J. Biomech., **24**(8), pp. 659–671.
[15] Abdel-Rahman, E. M., and Hefzy, M. S., 1998, "Three-Dimensional Dynamic Behavior of the Human Knee Joint under Impact Loading," Med. Eng. Phys., **20**, pp. 276–290.
[16] Tumer, S. T., and Engin, A. E., 1993, "Three-Body Segment Dynamic Model of the Human Knee," J. Biomech. Eng., **115**, pp. 350–356.
[17] Ling, Z.-K., Guo, H.-Q., and Boersma, S., 1997, "Analytical Study on the Kinematics and Dynamic Behaviors of a Knee Joint," Med. Eng. Phys., **19**(1), pp. 29–36.
[18] Blankevoort, L., Kuiper, J. H., Huiskes, R., and Grootenboer, H. J., 1991, "Articular Contact in a Three-Dimensional Model of the Knee," J. Biomech., **24**(11), pp. 1019–1031.

[19] Hefzy, M. S., Yang, H., Abdel-Rahman, E. M., and Alkhazim, M., 1997, ''Effects of Knee Flexion Angle and Quadriceps Contraction on Hamstrings Co-Contraction,'' Biomed. Eng. Appl. Basis Commun., **BED-36**, pp. 145–146.
[20] Hefzy, M. S., and Yang, H., 1998, ''Effects of Posterior Cruciate Insufficiency on Tibio-femoral and Patello-Femoral Contact Forces During Isometric Co-Contraction of the Quadriceps and Hamstrings,'' *Transactions of the 44th Annual Orthopaedic Research Society Meeting*, **23**(2), pp. 1034.
[21] McGinty, G., Irrgang, J. J., and Pezullo, D., 2000, ''Biomechanical considerations for rehabilitation of the knee,'' Clin. Biomech. (Los Angel. Calif.), **15**, pp. 160–166.
[22] Grood, E. S., Suntay, W. J., Noyes, F. R., and Butler, D. L., 1984, ''Biomechanics of the Knee Extension Exercise,'' J. Bone Jt. Surg., **66A**, pp. 725–733.
[23] Grood, E. S., and Suntay, W. J., 1983, ''A Joint Coordinate System for the Clinical Description of the Three-Dimensional Motions: Applications to the Knee,'' J. Biomed. Eng., **105**, pp. 136–144.
[24] Mow, V. C., Athesian, G. A., and Spilker, R. L., 1993, ''Biomechanics of Diarthrodial Joints: A Review of Twenty Years of Progress,'' J. Biomech. Eng., **115**, pp. 460–467.
[25] Thambyah, A., Thiagarajan, P., and Goh, J. C. H., 2000, ''Biomechanical Study on the Effect of Twisted Human Patellar Tendon,'' Clin. Biomech. (Los Angel. Calif.), **15**, pp. 756–760.
[26] Brenan, K. E., Campbell, S. L., and Petzold, L. R., 1989, *Numerical Solution of Initial-Value Problems in Differential-Algebraic Equations*, North-Holland, Elsevier Science Publishing Co., Inc.
[27] Petzold, L. R., 1983, ''A Description of DASSL: A Differential/Algebraic System Solver,'' In: Stepleman, R. S., Carver, M., Peskin, R., and Vichnevetsky, A., editors, Scientific Computing: Volume 1, IMACS transactions on scientific computation. Amsterdam-New York-Oxford: North Holland Pub. Co., pp. 65–68.
[28] Yasuda, K., Erickson, A. R., Johnson, R. J., and Pope, M. H., 1992, ''Dynamic strain behavior in the medial collateral and anterior cruciate ligaments during lateral impact loading,'' Trans. Orthop. Res. Soc., **17**, pp. 127.
[29] Shoemaker, S. C., Adams, D., Daniel, D. M., and Woo, S. L.-Y., 1993, ''Quadriceps/Anterior Cruciate Graft Interaction: An in Vitro Study of Joint Kinematics and Anterior Cruciate Ligament Graft Tension,'' Clin. Biomech. (Los Angel. Calif.), **294**, pp. 379–390.
[30] Biden, E., O'Connor, J., and Goodfellow, J., 1984, ''Tibial Rotation in the Cadaver Knee,'' *Transactions of the 30th Meeting of the Orthopaedic Research Society*, pp. 30.
[31] FitzPatrick, D. P., 1989, ''Mechanics of the Knee Joint,'' D.Phil. Thesis, Univ. of Oxford.
[32] Wilson, D. R., Feikes, A. B., Zavatsky, A. B., and O'Connor, J. J., 2000, ''The Components of Passive Knee Movement are Coupled to Flexion Angle,'' J. Biomech., **33**, pp. 465–473.
[33] Race, A., and Amis, A. A., 1994, ''The Mechanical Properties of the Two Bundles of the Human Posterior Cruciate Ligament,'' J. Biomech., **27**(1), pp. 13–24.
[34] Grood, E. S., Hefzy, M. S., and Lindenfield, T. N., 1989, ''Factors Affecting the Region of the Most Isometric Femoral Attachments. Part I: The Posterior Cruciate Ligament,'' Am. J. Sports Med., **17**(2), pp. 197–207.
[35] Hefzy, M. S., and Grood, E. S., 1986, ''Sensitivity of Insertion Locations on Length Pattern of Anterior Cruciate Ligament Fibers,'' ASME J. Biomech. Eng., **108**, pp. 73–82.
[36] Rovick, J. S., Reuben, J. D., Schrager, R. J., and Walker, P. S., 1991, ''Relation between Knee Motion and Ligament Length Patterns,'' Clin. Biomech. (Los Angel. Calif.), **6**, pp. 213–220.
[37] Wilk, K. E., Escamilla, R. F., Fleisig, G. S., Barrentine, S. W., Andrews, J. R., and Boyd, M. L., 1996, ''A Comparison of Tibiofemoral Joint Forces and Electromyographic Activity During Open and Closed Kinetic Chain Exercises,'' Am. J. Sports Med., **24**(4), pp. 518–527.
[38] Hirokawa, S., Solomonow, M., and Lu, Y., 1992, ''Anterior-Posterior and Rotational Displacement of the Tibia Elicited by Quadriceps Contraction,'' Am. J. Sports Med., **20**, pp. 299–306.
[39] Kaufman, K. R., An, K. N., Litchy, W. J., Morrey, B. F., and Chao, E. Y., 1991, ''Dynamic Joint Forces During Knee Isokinetic Exercise,'' Am. J. Sports Med., **19**, pp. 305–316.
[40] Walker, P. S., and Hajek, J. V., 1972, ''The Load Bearing Area in the Knee Joint,'' J. Biomech., **5**, pp. 581–589.
[41] Cheng, C. K., 1988, ''A Mathematical Model for Predicting Bony Contact Forces and Muscle Forces at the Knee During Human Gait,'' Ph.D. Dissertation. Iowa City (IA): The University of Iowa.
[42] Morrison, J. B., 1970, ''The Mechanics of the Knee Joint in Relation to Normal Walking,'' J. Biomech., **3**, pp. 51–61.
[43] Van Eijden, T. M., Kouwenhoven, E., Verbury, J., and Weijs, W. A., 1986, ''A Mathematical Model of the Patellofemoral Joint,'' J. Biomech., **21**, pp. 17–22.
[44] Gill, H. S., and O'Connor, J. J., 1996, ''A Biarticulating 2-Dimensional Model of the Human Patellofemoral Joint,'' Clin. Biomech. (Los Angel. Calif.), **11**(2), pp. 81–89.
[45] Ahmed, A. M., Burke, D. L., and Yu, A., 1983, ''In Vitro Measurement of Static Pressure Distribution in Synovial Joints-Part II: The Retropatellar Surface,'' J. Biomech. Eng., **105**, pp. 226–236.
[46] Buff, H., Jones, L. C., and Hungerford, D. S., 1988, ''Experimental Determination of Forces Transmitted through the Patellofemoral Joint,'' J. Biomech., **21**, pp. 17–22.
[47] Hille, E., Schulita, K. P., Henrichs, C., and Schneider, T., 1985, ''Pressure and Contact-Surface Measurements within the Femoro-Patellar Joint and their Variations Following Lateral Release,'' Arch. Orthop. Trauma Surg., **104**, pp. 275–282.
[48] Hefzy, M. S., Jackson, W. T., Saddemi, S. R., and Hsieh, Y. F., 1992, ''Effects of Tibial Rotations on Patellar Tracking and Patello-Femoral Contact Areas,'' J. Biomed. Eng., **14**, pp. 329–343.
[49] Hehne, H. J., 1990, ''Biomechanics of the Patellofemoral Joint and Its Clinical Relevance,'' Clin. Orthop. Relat. Res., **258**, pp. 73–85.
[50] Cohen, Z. A., Roglic, H., Grelsamer, R. P., Henry, J. H., Levine, W. N., Mow, V. C., and Ateshian, G. A., 2001, ''Patellofemoral Stresses During Open and Closed Kinetic Chain Exercises,'' Am. J. Sports Med., **29**(4), pp. 480–487.
[51] Takeuchi, R., Koshino, T., Saito, T., Suzuki, E., and Sakai, N., 1999, ''Patello-Femoral Contact Area and Compressive Force after Anteromedial Displacement of Tibial Tuberosity in Amputated Knees,'' The Knee, **6**, pp. 109–114.
[52] Moeinzadeh, M. H., Engin, 1988, ''Dynamic Modeling of the Human Knee Joint,'' In: Computational Methods in Bioengineering, *Proceedings of the 1988 WAM*. Chicago (IL): ASME; BED-Vol. **9**, pp. 145–156.